Spring 2015

Laser surface and sub-surface repair during metal additive manufacturing

Prudvi Teja Ravi

Department:

LASER SURFACE AND SUB-SURFACE REPAIR DURING METAL ADDITIVE MANUFACTURING

By

PRUDVI TEJA RAVI

A THESIS

Presented to the Faculty of Graduate School of

MISSOURI UNIVERSITY OF SCIENCE AND TECHNOLOGY

In Partial Fulfillment of the Requirement for the Degree

MASTERS OF SCIENCE IN MANUFACTURING ENGINEERING

2015

Approved by

Dr. Frank Liou

Dr. Edward C Kinzel

Dr. Heng Pan

ABSTRACT

This study examines the use of laser surface treatment to repair surface and subsurface defects. Numerical analysis was performed on laser surface melting using Gaussian heat distribution equations to analyze the depth of the melt pool created by the phenomena. Concurrently, a process map was developed with a planned set of experiments by varying the ranges of laser power and travel speed to determine the dimensions of the melt pool across the gamut. The data generated from both the process studies and the numerical analysis was then used to determine the ideal operating ranges of the process parameters to repair surface and subsurface defects. These parameters were then used to validate the repair of surface and subsurface defects of varying dimensions artificially created on stainless steel 304 substrates. The surfaces of these repaired samples were topologically mapped to geometrically assess and quantify the repair achieved. Measured standard deviations of these topological profiles before and after the repair have shown that the laser surface treatment can be used as a viable option for repair of surface imperfections. After completing the surface study the samples were cross-sectioned to volumetrically analyze the internal regions for the occurrence of voids. This final part of research justified the ability of the laser surface treatment in the repair of sub-surface defects. This work has successfully repaired surface defects of sizes of 1mm*1mm*1mm and has identified the ideal process parameters needed to achieve successful repair. It has also led to successful repair of 0.2mm-0.6mm size subsurface defects up to depths of 0.5mm.

ACKNOWLEDGMENTS

I would like to express my gratitude to my advisor, Dr. Frank Liou. His guidance, expertise and remarks were vital throughout my work. I would also like to thank my other committee members Dr. Edward C. Kinzel and Dr. Heng Pan for their time and advice on my work.

I would like to thank Sriram Praneeth Isanaka, Wei Le and Todd Sparks for their guidance with numerical aspects of this work. I would like to thank the members of the LAMP lab for their willingness to help throughout my work.

Finally, I would like to thank my parents Rambabu Ravi and Mytreyi Ravi and my brother Ravi Teja Ravi for their endless love and support.

TABLE OF CONTENTS

LIST OF ILLUSTRATIONS

Page

LIST OF TABLES

Page

1. INTRODUCTION

1.1. OBJECTIVE

Over the last couple of decades Laser Surface Melting (LSM) has gained popularity as a novel surface modification method in the treatment of metals. It is a process where the material surface is melted by scanning the surface of existing components with a laser beam to locally alter the topology and micro-structures. One of the advantages of employing lasers is the extremely high cooling rates that can be achieved which radically alter the local geometry and microstructures in the affected regions. This effect of lasers is used by LSM to produce refined microstructures by rapidly melting and the subsequent solidification of the melted zones [1]. The study in this thesis is aimed at the ability of LSM to be used as a repair option for surface and subsurface defeats. To experimentally validate the repair-ability of LSM, a 1kW fiber laser was used to repair defects of varying dimensions and depths on stainless steel 304 (SS304) substrates.

Around the world, a significant amount of work has been done on studying the microstructure and mechanical properties of laser surface melted SS304. Studies have shown that laser surface melting produces improved pitting corrosion resistance in SS304 [2]. LSM samples of SS304 have also shown significant increase in wear resistance and hardness properties of the surface layer post heat treatment [3]. The objective of this study is to utilize LSM to repair surface and subsurface defects using factors that most affect the repair-ability namely the depth and size of the melt pool and their controlling process parameters. The basic principle behind successful repair is the relation between

the energy input from the source and it's interaction with the local geometry at the point of impact on the substrate. By utilizing a moving laser source the research hypothesizes that the melted material will recrystallize to fill the defect and improve local topology. The same principle can be applied to subsurface defects although it is theorized that their surface topology will still read like a defect.

1.2. BACKGROUND

Cabeza et al. proposed the concept of repairing damaged surfaces of steel using LSM [3]. A high power Nd-YAG laser was used to melt the surface of steel in different thermal situations. The steel was initially heat treated by varying temperatures to mimic the mechanical properties of maraging steel. During this study they observed a significant increase in the hardness properties and wear resistance of the surface layer. Pinkerton et al. tried to use diode laser metal deposition process as a repairing tool [4] by trying to repair rectangular and triangular cross-sectional slots. Their statistical analysis varied laser power, power mass flow rate and traverse speed to numerically quantify repair. While they achieved repair in certain cases their work was plagued by the consistent creation and retention of porosity. The surface slot exhibited poor fusion characteristics with incoming powder as the geometry of their side wall shielded the incoming power from absorbing the laser. Also the V-slots had porosity issues at their base due to the sharp angles created by the slot. They observed increasing porosity with increasing laser power or powder flow.

1.3. THEORETICAL LASER SURFACE MELTING RELATIONSHIPS

Literature provided an excellent start point for this research by detailing the relationship between the process parameters as numerical models. These numerical methods as seen in Figure 1-1 can be used to simulate the process of heat and fluid flow of a moving melt pool and its relation to the process parameters [1]. To determine the effects of laser power, beam size and feed rate (travel speed) on the depth of the melt zone, graphs depicting the relation between beam power and traverse rate were used. The normalized beam power (dimensionless) and normalized traverse rate (dimensionless) indicate the melt depths. Their relationship is shown in equations 1 and 2.

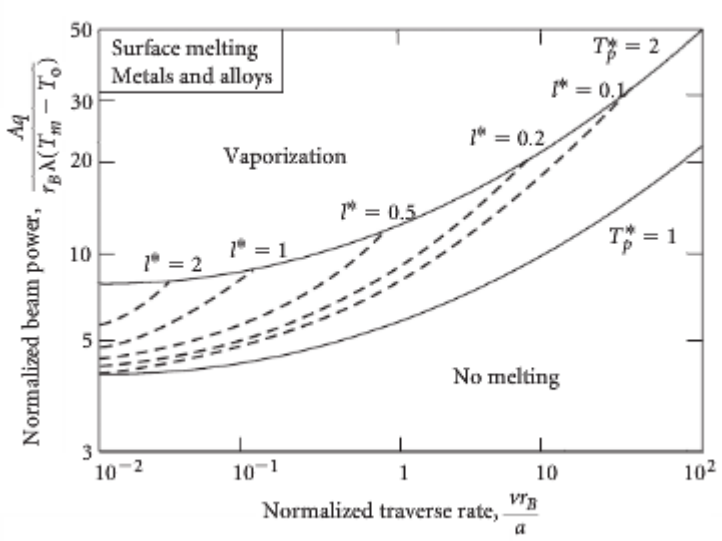

Figure 1-1 Laser surface melting diagrams [1]

$$\text{Normalized Power} = \frac{\text{Aq}}{r_B\lambda(T_m - T_o)} \quad (1)$$

$$\text{Normalized traverse rate} = \frac{\text{v}r_B}{a} \quad (2)$$

where

A is the absorptivity of the material,

q is the laser power,

r_B is the radius of the laser beam,

λ is thermal conductivity,

T_m is the melting temperature,

T_o is room temperature,

v is the feed rate (travel speed) and

a is the thermal diffusivity of material.

After calculating the two values, the depth of the melt pool can be estimated from the graph. For this research the minimum depth of the melt pool was estimated to be between 0.2 mm – 0.3 mm for different process conditions of laser power and travel speed.

1.4. NUMERICAL ANALYSIS

Based on the literature reviewed, in-house numerical solutions were proposed and developed to gain greater insight into LSM and the results are detailed in the forthcoming sections. A laser beam is a concentrated heat source that is modelled using a Gaussian distribution [5]. Its numerical solution was generated using

$$q(r) = \frac{fQ}{\pi {r_o}^2} \exp\left(-f \frac{r^2}{{r_o}^2}\right). \quad (3)$$

where Q is the laser beam power [W], r_o is radius of the laser beam, r is the current radius[m] and f is the coefficient (for the sake of this research is assumed as 3). The laser beam power distribution shape may vary from the equation 3. By adding exponent's n1

and n2 into the equation 3, changes in the shape of the heat source power distribution can be obtained [5, 6].

$$q(r) = \frac{3Q}{\pi {r_o}^2} \exp(-3(\frac{x}{r_o})^{n1} - 3\left(\frac{y}{r_o}\right)^{n2}). \quad (4)$$

where x and y are the co-ordinates, n1 and n2 will be equal to 2 for a typical Gaussian model [5].Since the current model is 2 dimensional, the numerical value of y is 0 and with both y and r_o having the same dimensions this would not have any impact on the equation. Subsequently the resultant equation reduces to

$$q(r) = \frac{3Q}{\pi {r_o}^2} \exp(-3\left(\frac{x}{r_o}\right)^2). \quad (5)$$

The mesh used to perform the analysis can be seen in the Figure 1-2 Numerical analysis of a moving heat source was performed in FLUENT. A user subroutine was created to incorporate above equation and laser parameters in the numerical model.

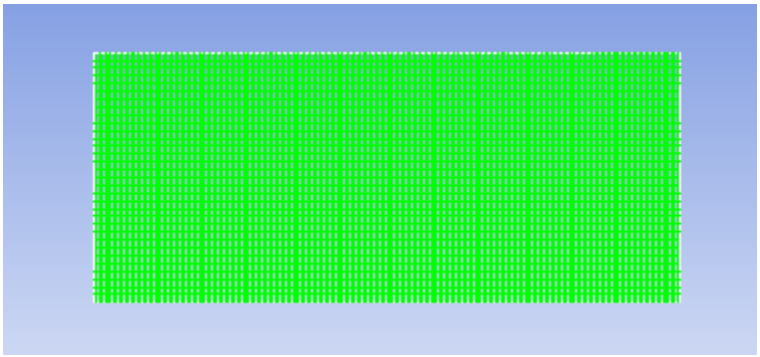

Figure 1-2 Mesh of 2D sample

A 2D geometric model of dimensions 15*6.35mm was created and meshed using ICEMCFD. The initial conditions for the model are assumed to be transient along with boundary conditions for energy, solidification and melting models for SS304. All the four walls were initialized at 300K. The heat flux on left, right and bottom walls were held at

0 while the heat flux on the top was based on the Gaussian distribution model. The solver was initialized and the solution compiled to determine the heat dissipation. The result of the analysis shows the liquid fraction present which was used to determine the melt pool depth.

1.5. CONDITIONS FOR GAS PORE ESCAPE

The thermo-capillary forces influenced by the relative laser motion (surface tension) has a tendency to facilitate melt pool dynamics. Therefore any porosity present in the material tends to move and escape during the molten phase. There are various factors that affect gas pore dynamics including solidification velocity and gas bubble velocity [7].

1.5.1. Solidification Velocity. Determined by the depth of the melt pool, length of tail and feed rate (table speed).

V_s = (Melt pool Depth * feed rate)/length of the tail (6)

1.5.2. Bubble Velocity. This is estimated relative to all the forces acting on the bubble namely the convective fluid flow, buoyancy and thermo-capillary force [3]. The sum of all the velocity components of these forces is calculated as

$V_b = V_c + V_t + V_{bu}$ (7)

where V_c is velocity component of convective fluid flow, V_{bu} is the velocity component of the buoyancy and V_t is the velocity component of thermo-capillary force.

Triantafyllidis et al. [7] computed this velocity to be

$$V_b = \frac{q_a r}{\mu k}\frac{d\sigma}{dT} + \frac{R}{2\mu}\frac{d\sigma}{dT}\frac{dT}{dz} + \frac{R^2 g\rho}{3\mu} \quad (8)$$

The dynamics of the gas pore is governed by its relative velocity which can be estimated by subtracting equation 8 (velocity of the bubble) and equation 6 (solidification velocity) as shown in equation 9.

Relative velocity of bubble = Velocity of bubble – Solidification velocity

$$V_R = V_b - V_s \quad (9)$$

If the calculated $V_r > 0$, the gas pore escapes the melt pool, while if $V_r < 0$, the gas pore does not have the energy to escape and remains trapped.

1.5.3 Calculations. When the laser scans the metal surface, the pore will be inside the melt pool. After laser melting the initial force that acts on pore it is the buoyancy force. Assuming that the pore is filled with air and including its properties into equation 8, the velocity of the pore is calculated. In an ideal repair condition the gas pore must escape, and this can only be achieved if the bubble velocity exceeds the solidification velocity. The least solidification velocity that's practically achievable is when the maximum laser power is 1000W and minimum feed rate is 100mm/min. From all of these values the final solidification velocity was computed to be 0.38mm/sec. Therefore, for the bubble to initially move towards the surface the velocity component due to buoyancy should be greater than 0.38mm/sec. From equation 8 we understand that the velocity of a pore due to buoyancy will be dependent upon the radius, density and dynamic viscosity. By assuming that the pore is filled with air, the only factor that has influence on the relative velocity is the size of the pore. Therefore, smaller is the size of the pore, smaller will be the velocity of its upward motion. By using the properties of air (density of pore 0.19 kg/m^3 and the dynamic viscosity to be 6×10^{-5}) and a pore of 0.6 mm size, the velocity of the bubble is calculated as 1mm/sec. Upon calculation, the

velocity of the pore will be less than the solidification velocity of 0.38 which is the minimum for our system will be when the pore size is less than 350 microns. Therefore, if the pore is less than 350 microns in size the pore will not reach the surface. Once the bubble reaches the surface, the thermo-capillary force and forces due to convective heat flow will start to act. The velocity component of these forces cannot be estimated.

2. EXPERIMENTAL SETUP

2.1. MATERIAL

SS 304, an austenitic, chromium-nickel stainless steel having low carbon content and high chromium and nickel content is chosen as substrate material. It has good performance in deep drawing, cold forming, spinning and rolling due to its homogeneous structure, high ductility and excellent strength. It is generally nonmagnetic and slightly magnetic in cold worked condition. The chemical composition of SS 304 can be seen in the below Table 2.1.

Table 2.1 Chemical composition of 304 stainless steel

C	Cr	Fe	Mn	Ni	P	S	Si
0.08	18-20	66.3-74	2	8-10.5	0.045	0.03	1

2.2. DESIGN OF EXPERIMENTS (DOE)

To determine the depth of the melt pool experimentally a DOE is performed with two factors affecting the depth of the melt pool, namely laser power and travel speed**.** The laser surface melting diagrams were initially used to determine the range of laser power and travel speed. The laser employed for the research is a 1000 W fiber laser. The upper and lower limit of the factors were chosen to ensure that they had an ability to form and sustain a melt pool. To determine the minimum laser power, it was assumed that the minimum melt pool depth should be between 200-300 microns (assumed from the sizes

of defects to be repaired). Based on this assumption, 400W was selected from the results generated from the laser surface melting diagrams. The lower limit of the travel speed for the laser's unhindered function was determined to be 100 mm/min. To determine the upper limit of travel speed based on the laser surface melting diagrams it was determined that 400 mm/min should be the maximum speed to attain the 200-300 micron melt pool depths for 1000 W laser power.

A 2^3 factorial design of experiment was implemented by varying the above factors for three levels. The laser power is varied between 400W, 700W, and 1000W while the travel speed varies between 100mm/min, 250 mm/min, and 400mm/min. The list of the design of experiments can be seen in the below Table 2.2.

Table 2.2 List of experiments in DOE

S.No	**Travel Speed (mm/min)**	**Laser Power (Watts)**
1	100	1000
2	100	700
3	100	400
4	250	1000
5	250	700
6	250	400
7	400	1000
8	400	700
9	400	400

2.3. PRINCIPLE OF OPERATION AND EXPERIMENTAL SETUP

The laser used is a single mode CW ytterbium fiber laser system whose wavelength lies in the near infrared spectral range (1060-1080 nm). The laser spot size is approximately 2mm at a distance of 550mm focal length. The schematic of the laser system can be seen in the Figure 2-1**.** The SS 304 sample is surface treated using the laser system for a travel length of 15mm. The experiment is repeated on multiple samples based on the DOE seen in Table 2.2. A schematic diagram of the laser surface melting can be seen in the Figure 2-2.

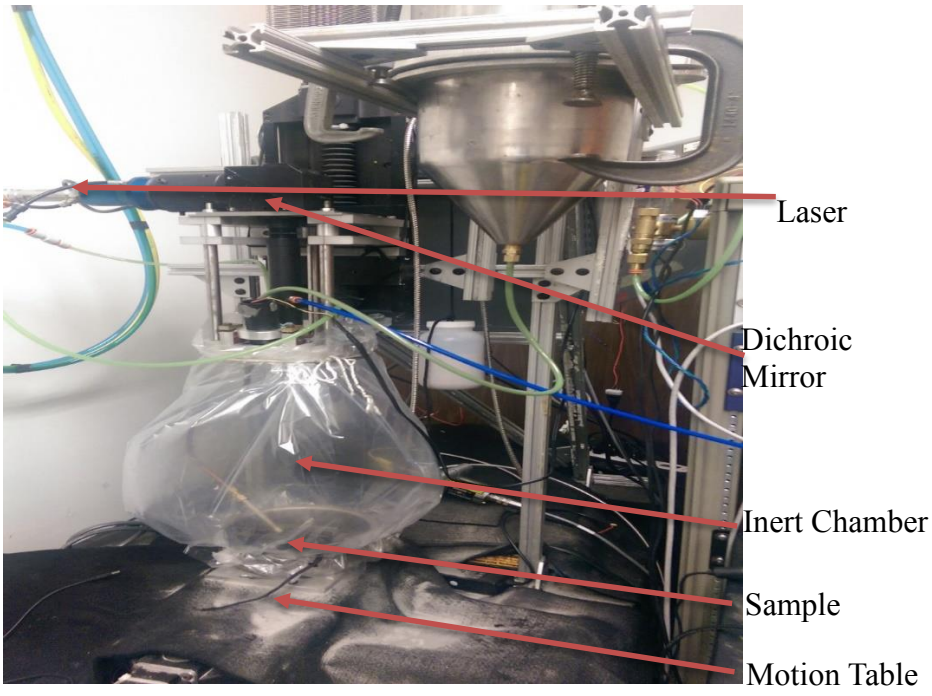

Figure 2-1 Experimental setup

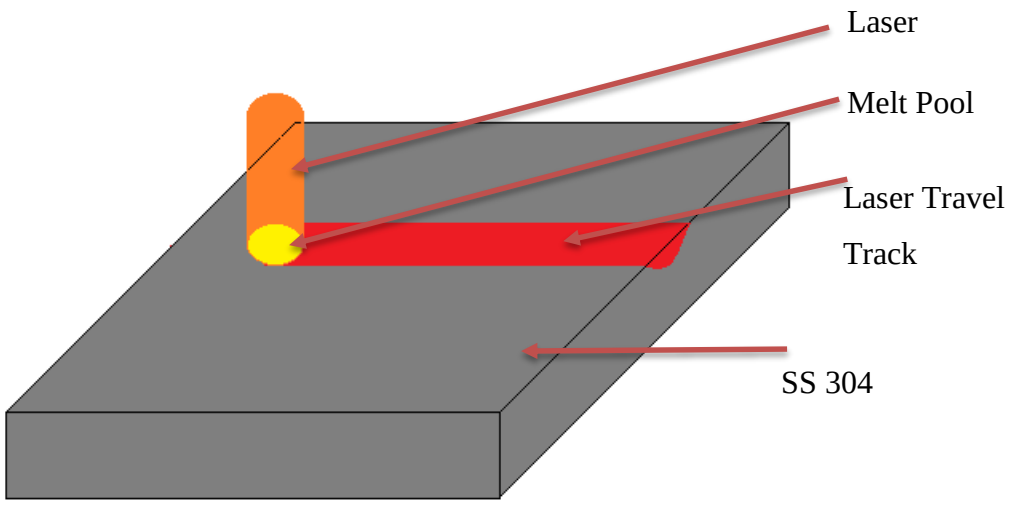

Figure 2-2 Laser surface melting

2.4. EXPERIMENTAL ESTIMATION OF MELT POOL DEPTH

Upon completion of the laser surface melting of the samples, they were cross-sectioned using a wire- Electrical Discharge Machine (EDM). These cut samples were mounted in bakelite. The samples were systematically ground and polished to 0.5 micron surface finish. The polished samples were etched using Marbles reagent (mixture of copper sulphate and hydrochloric acid). Optical microscopy was conducted on the etched sample to distinguish the melt pool boundary and heat affected zones and thereby calculate the depth of the melt pool.

2.5. SAMPLE PREPARATION

The samples needed for experimental validation were made of uniform dimensions with the same material which would act as a blocking factor to minimize the variation in this DOE. They are classified into surface and sub-surface samples and were made as discussed in this section.

2.5.1. Surface Defects. SS 304 specimens of 4”x1”x0.25” were prepared using a manual milling machine. The surface defects were created using a 1 mm end mill to drill a 1 mm and 0.5 mm deep hole into the sample as shown in the Figure 2-3. An optical image indicating the topological map of the hole is shown in Figure 2-4.

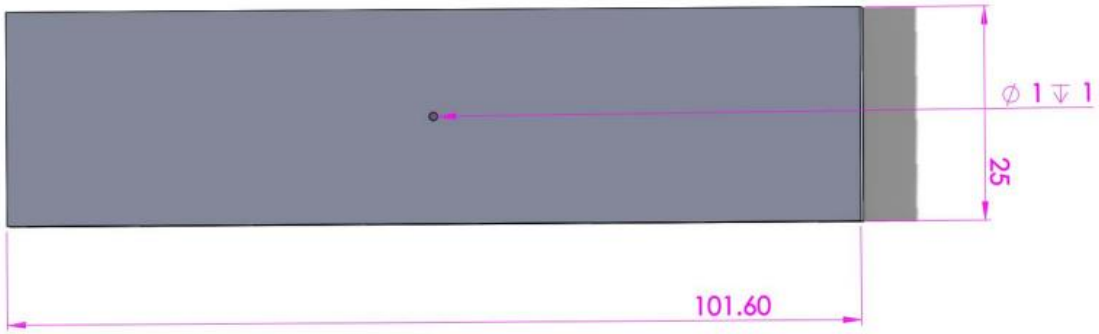

Figure 2-3 Computer aided design (CAD) model of surface defect (Top view)

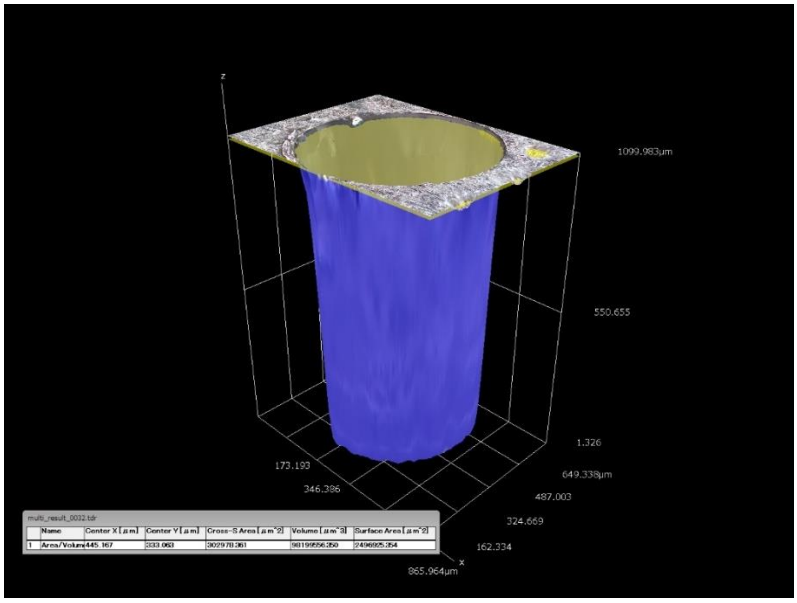

Figure 2-4 Optical image of the surface defect indicating its topology

2.5.2. Subsurface Defects. Specimens made of SS 304 of dimensions 0.5”x 4”x1” were prepared. Holes of sizes 200 microns, 400 microns and 600 microns were drilled from the side to a depth of 1mm. The CAD model of the hole can be seen in Figure 2-5 while Figure 2-6 shows an optical image with its topological profile. This sample was ground and polished to a 0.5 micron surface finish. A similarly prepared second sample was employed to cover the defect and prevent the gas bubbles from escaping through the side while simulating the bubble migrating to the top of the melt pool based on its buoyancy. The setup of both the samples fixed in the vice of the laser system can be seen in Figure 2-7.

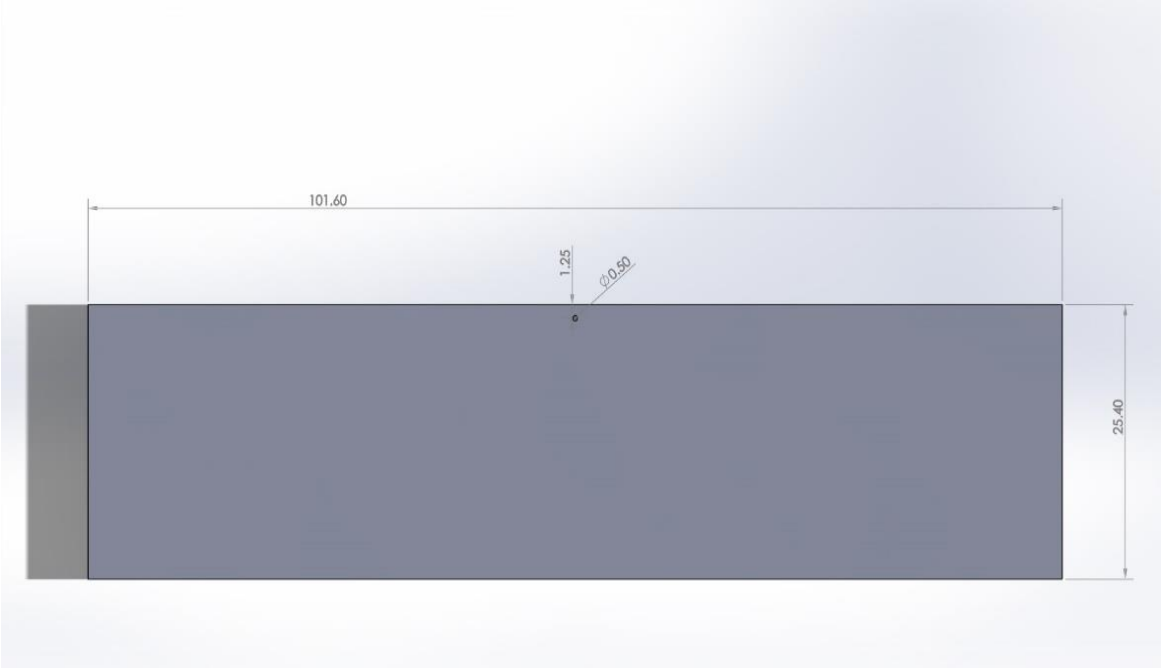

Figure 2-5 CAD model of subsurface defect (Front view)

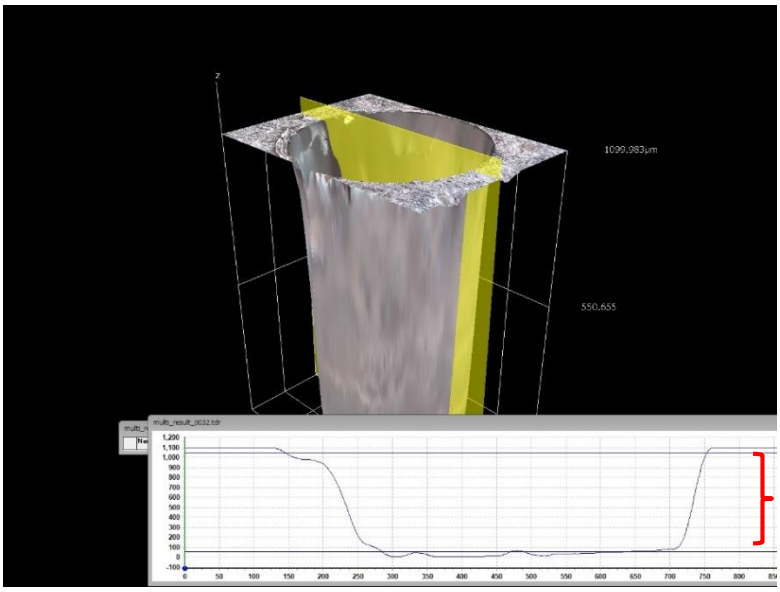

1mm deep pore

Figure 2-6 Microscopic 3D image of the subsurface defect

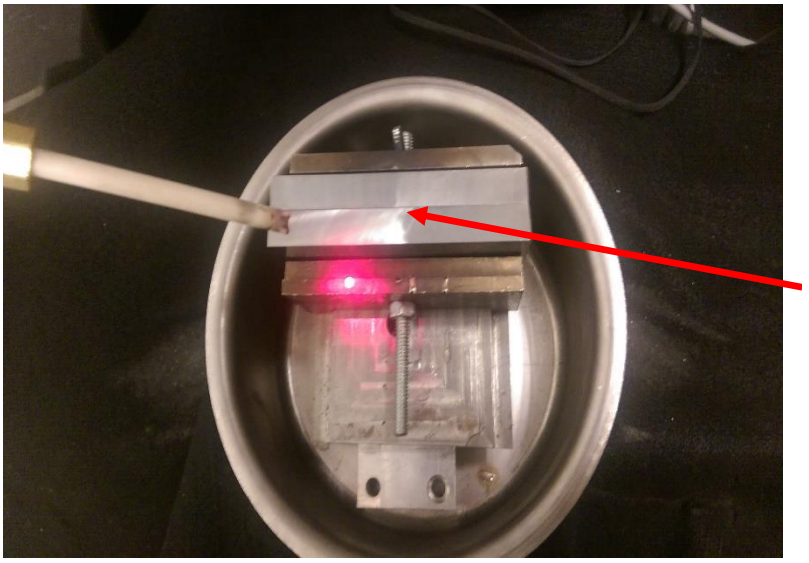

Figure 2-7 Setup of samples for subsurface repair

2.6. REPAIR

The data from the numerical analysis and the design of experiments was used to determine the laser power and travel speed parameters for repairing both surface and subsurface defects. LSM will be employed to repair the same by starting from a point located 7 mm before the defect and ending 7 mm after the defect to simulate 15 mm of travel. In the case of sub-surface repair the LSM will simulate three cases: a) exactly on the defect, b) at 0.5mm offset from defect and c) at 1mm offset from the defect.

2.7. SURFACE MAPPING

The repaired samples are surface mapped using an optical microscope to topologically quantify repair. The entire travel length was topologically mapped to assess the variation in the mean and standard deviation along the laser travel path. The zones including the defect section and areas preceding and subsequent are most vital to the quantification of repair. The repaired zones will be compared with baseline means and

standard deviation measured on a defect-less LSM sample. In both surface and subsurface repair the samples will be cross-sectioned using a wire-EDM to investigate the internal volumes for voids and validate the repair.

3. RESULTS

3.1. NUMERICAL ANALYSIS

The numerical analysis of LSM was performed on rectangular specimen of 15x6.35mm. The speed of the moving heat source was maintained at 100mm/min. The analysis was done for 3 different laser powers including 1kW, 0.7kW and 0.4kW. The delineation between the solid and liquid zones is determined based on the simulated liquid fraction shown in Figure 3-1, Figure 3-2 and Figure 3-3. The depths of the melt pools are tabulated in the Table 3.1.

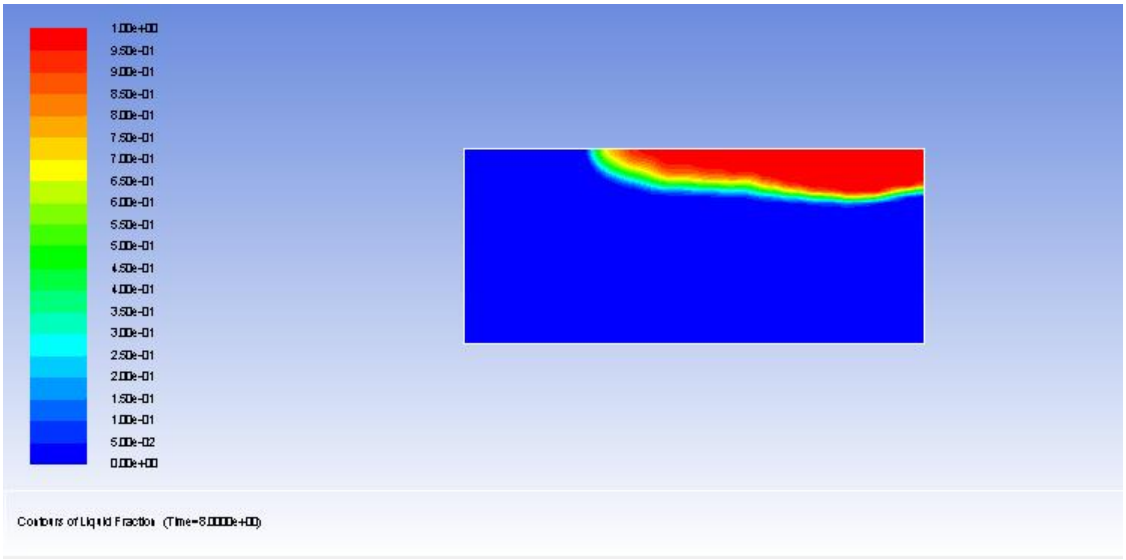

Figure 3-1 Melt pool depth for 1kW and 100mm/min

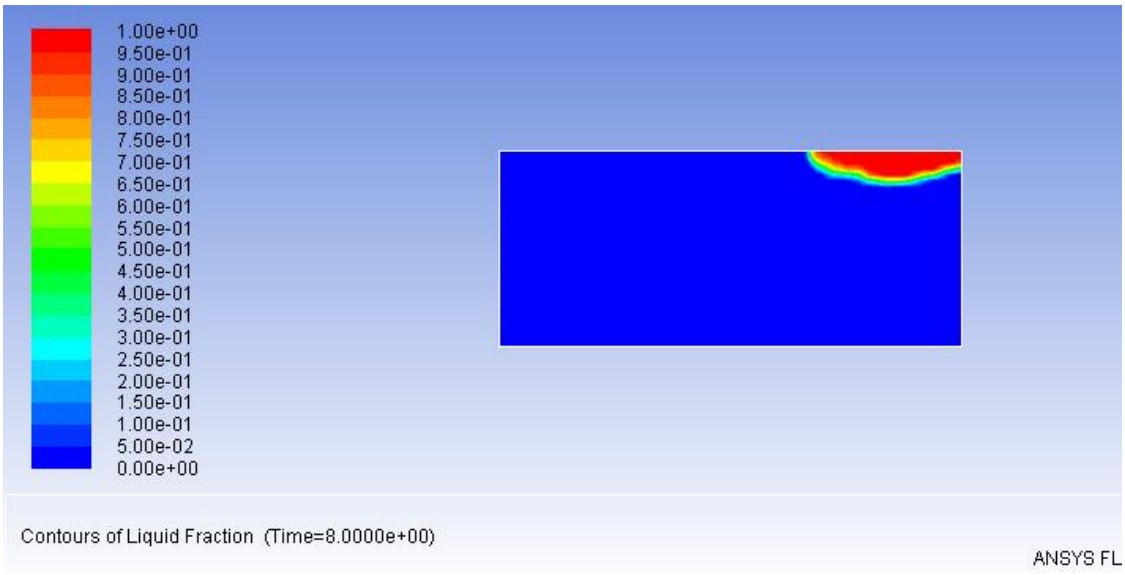

Figure 3-2 Melt pool depth for 700W and 100mm/min

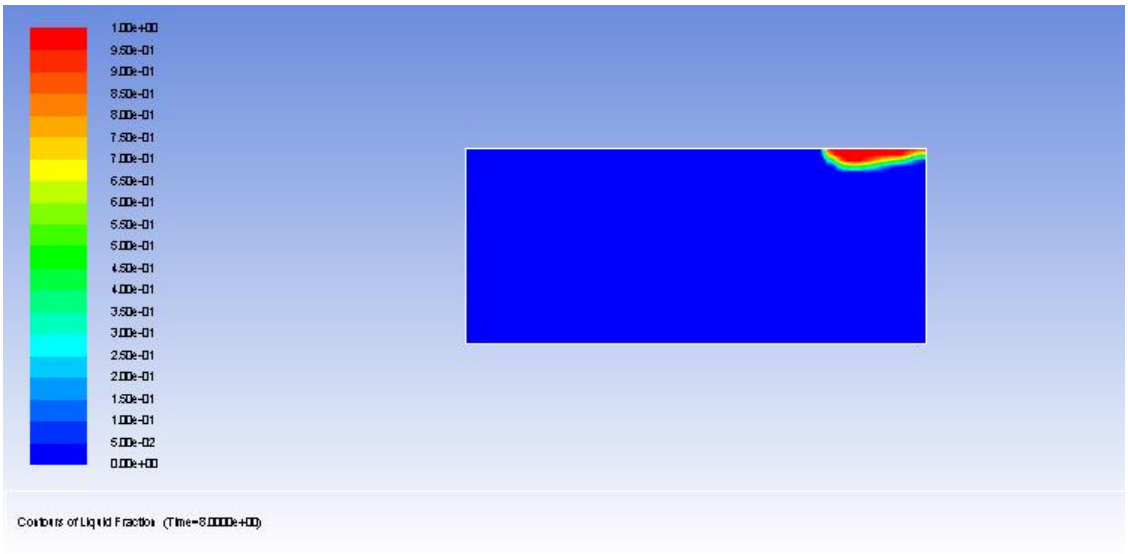

Figure 3-3 Melt pool depth for 400W and 100mm/min

Table 3.1 Melt pool depths for numerical analysis at different laser powers

Laser power(kW)	**Melt pool depth(mm)**
1	1.46
0.7	0.95
0.4	0.55

From the above table it can be observed that there was a steady increase in the melt pool depth with an increase in laser power. The result was along expected lines due to the fact that greater energy input translates into more energy per unit mass which ultimately leads to the formation of a larger melt pool based on the local heat transfer characteristics.

3.2. EXPERIMENTAL ANALYSIS

The depth of the melt pool was calculated by using the microscopy data of etched samples. The microscopic data of the depths of the melt pool can be seen from the Figure-3-4, Figure-3-5, Figure-3-6, Figure-3-7, Figure-3-8, Figure-3-9, Figure-3-10, Figure-3-11 and Figure3-12. The depths of the melt pools from the experimental analysis are tabulated in Table 3.2.

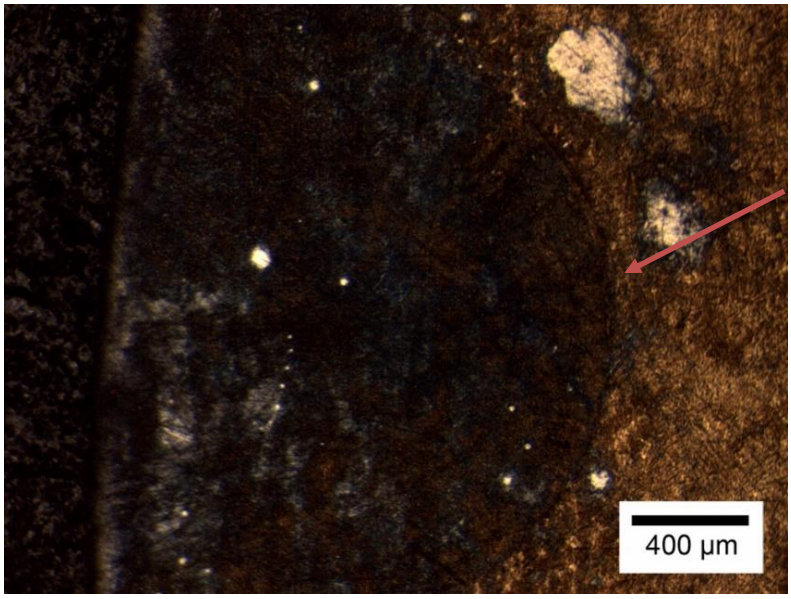

Figure 3-4 Microscopy of LSM sample at 1kW and 100mm/min travel speed

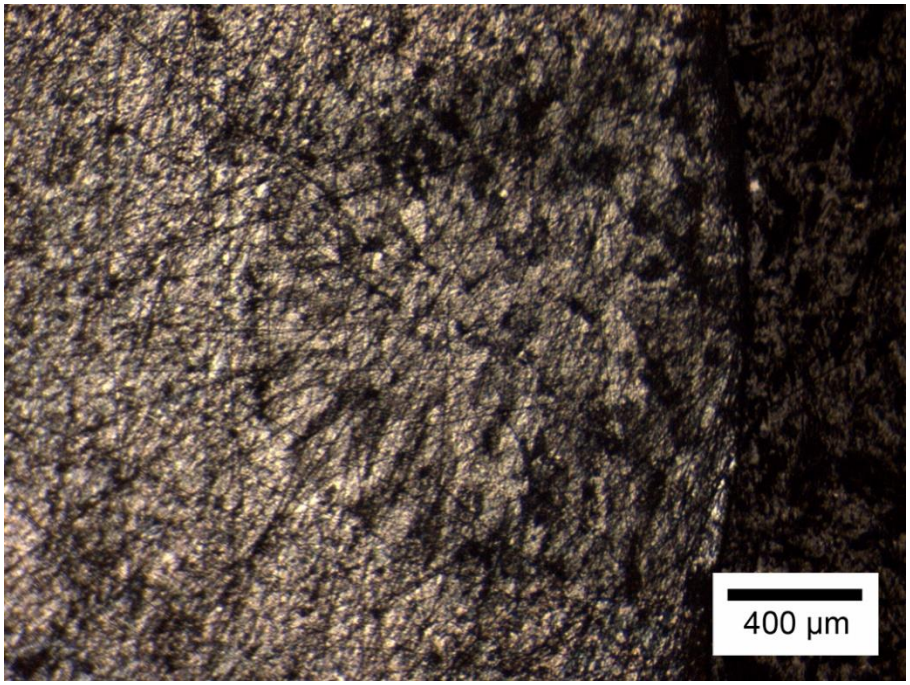

Figure 3-5Microscopy of LSM sample at 1kW and 250mm/min travel speed

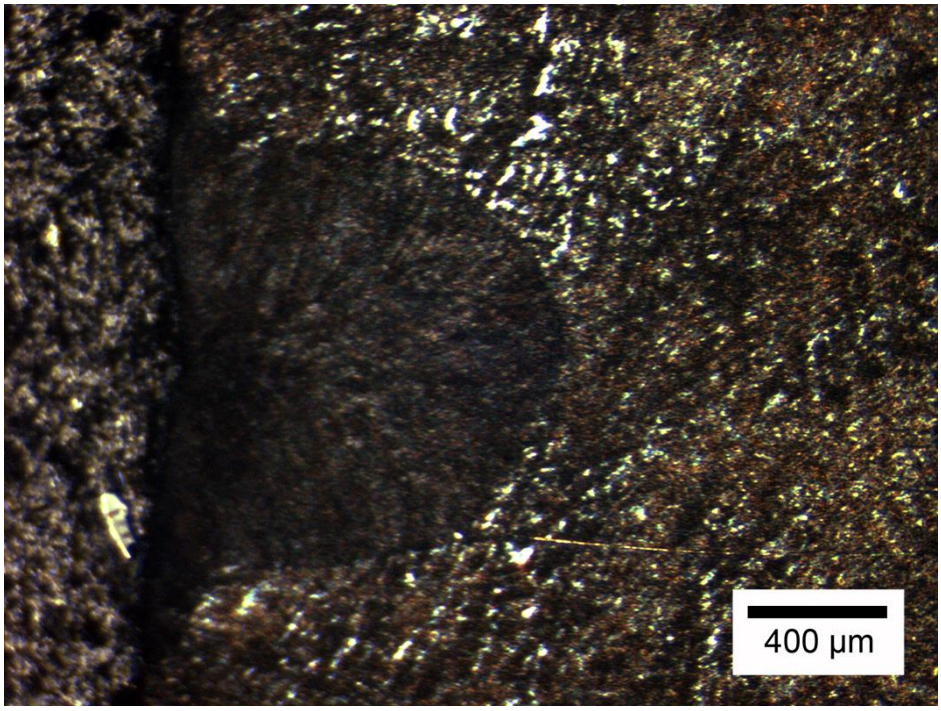

Figure 3-6Microscopy of LSM sample at 1kW and 400mm/min travel speed

Figure 3-7Microscopy of LSM sample at 0.7kW and 100mm/min travel speed

Figure 3-8Microscopy of LSM sample at 0.7kW and 250mm/min travel speed

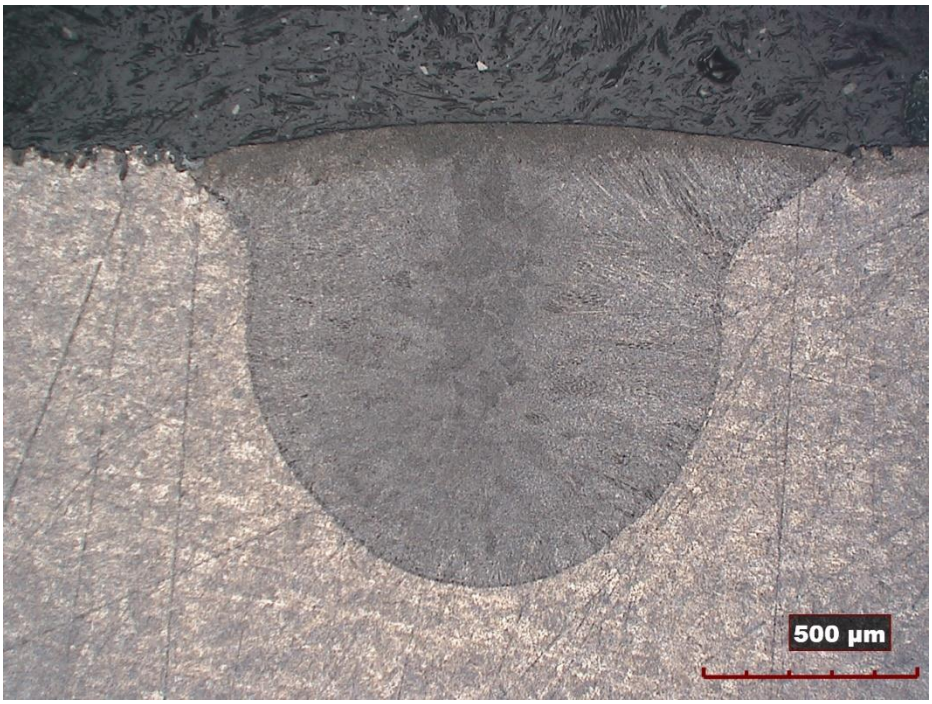

Figure 3-9Microscopy of LSM sample at 0.7kW and 400mm/min travel speed

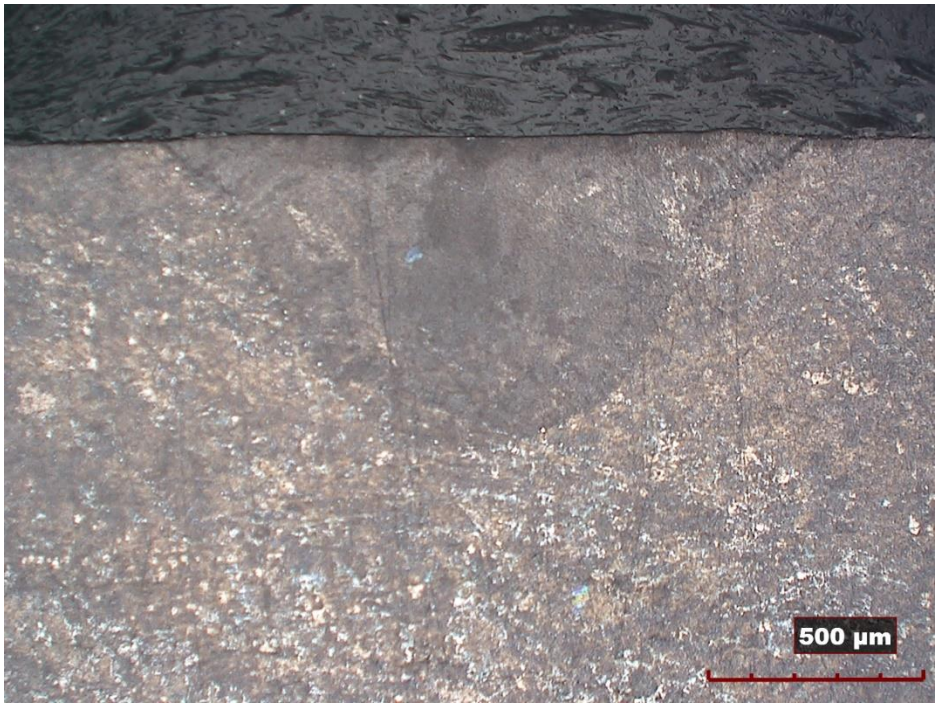

Figure 3-10Microscopy of LSM sample at 0.4kW and 100mm/min travel speed

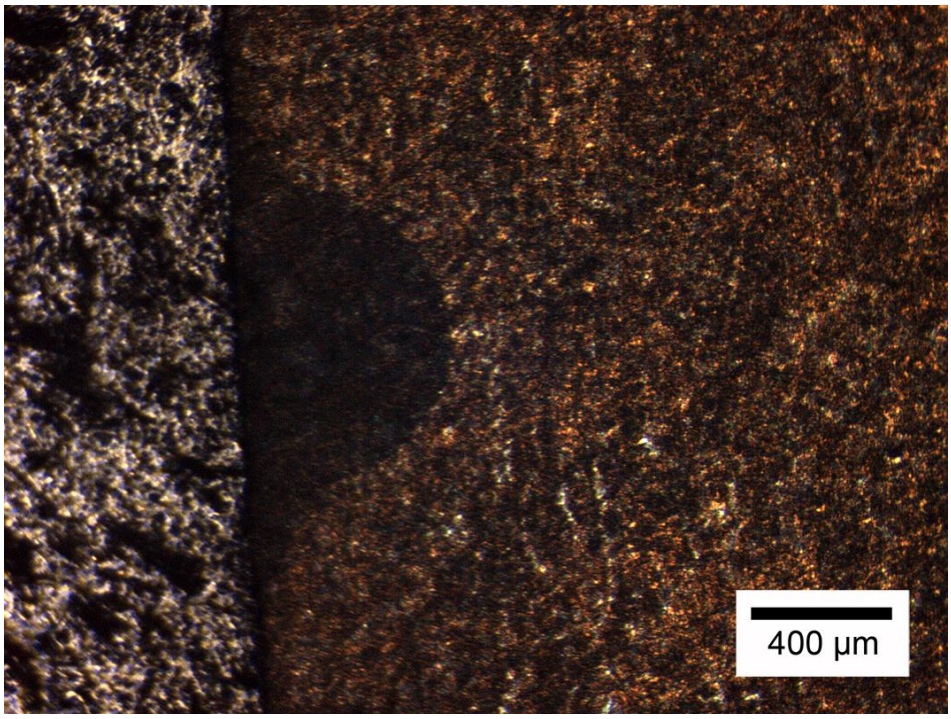

Figure 3-11Microscopy of LSM sample at 0.4kW and 250mm/min travel speed

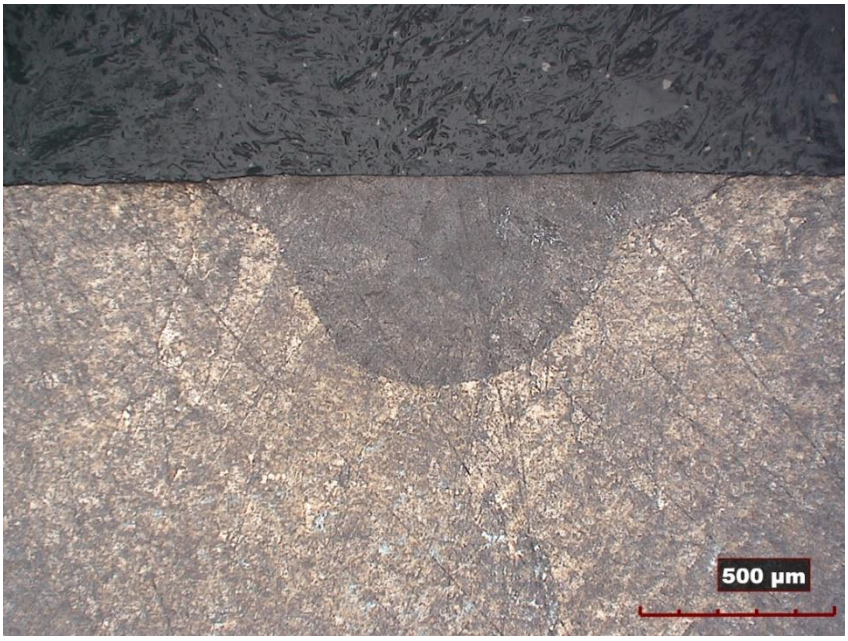

Figure 3-12Microscopy of LSM sample at 0.4kW and 400mm/min travel speed

Table 3.2 Melt pool depths for the design of experiments

Laser power (watts)	**Speed (mm/min)**	**Melt pool depth (mm)**
1000	100	1.695
1000	250	1.154
1000	400	0.890
700	100	1.127
700	250	0.920
700	400	0.814
400	100	0.661
400	250	0.525
400	400	0.480

From Table 3.2 it was observed the relationships between the process parameters followed proportional trends. While the melt pool depth increased with an increase in laser power, a travel speed increase reduced the melt pool depth. The results of the LSM repair were expected, owing to the fact that with increased energy input as the energy input to the substrate will increase with increase in laser power or decrease in travel speed.

3.3. COMPARISION BETWEEN NUMERICAL AND EXPERIMENTAL DATA

It was observed that the depth of the melt pool generated from the numerical analysis was lower than the observed values from the experimental data. The data from the experiments observed comparable trends with the numerical data which suggest the acceptable comparability. The comparison of experimental and numerical data can be seen from the Table 3.3

Table 3.3 Comparison of numerical and experimental data

Laser power (Watts)	**Numerical results (mm)**	**Experimental results (mm)**	**Variation**
1000	1.46	1.69	13.6%
700	0.95	1.13	15.9%
400	0.55	0.66	16.67%

From the above table it was observed that there has been a variation of 13-17% between the experimental and numerical results. It can be seen from the table that the least variation occurred at the highest energy input and the most variation was observed at the lowest energy input. This discrepancy is attributed to the larger volume of the melt pool created in the former situation which will lead to more distinguishable results.

3.4. SURFACE REPAIR

3.4.1 Repairing a Hole of Diameter 1mm and Depth of 1mm. Based on the data generated from the design of experiments and the numerical analysis 1kw laser and 250mm/min travel speed are theorized as the best values to repair this defect using LSM. The surface profile after the repair is as shown in Figure 3-13.

The repaired sample was analyzed with a higher resolution lens at three locations, a) before the defect, b) on the defect and c) after the defect. The length of each zone is 2000 microns, for a total of 6000 microns. In each of these three cases mean and standard deviation of the points the locations is calculated and compared. Similar analysis is performed on defect free laser surface melted SS 304 sample. The means and standard deviations are calculated for a these two samples and compared with the repaired sample. The results are tabulated as shown in the Table 3.4. It was observed that the standard deviations of the repaired samples were comparable with that of the defect free laser surface melted sample which indicate successful repair. Once the surface analysis of the repaired specimens were done, the samples were sectioned to check internal repair characteristics. The internal surface showed no presence of pores which suggest that the repair characteristics were excellent. The repair can be seen in the Figure 3-14 and Figure 3-15.

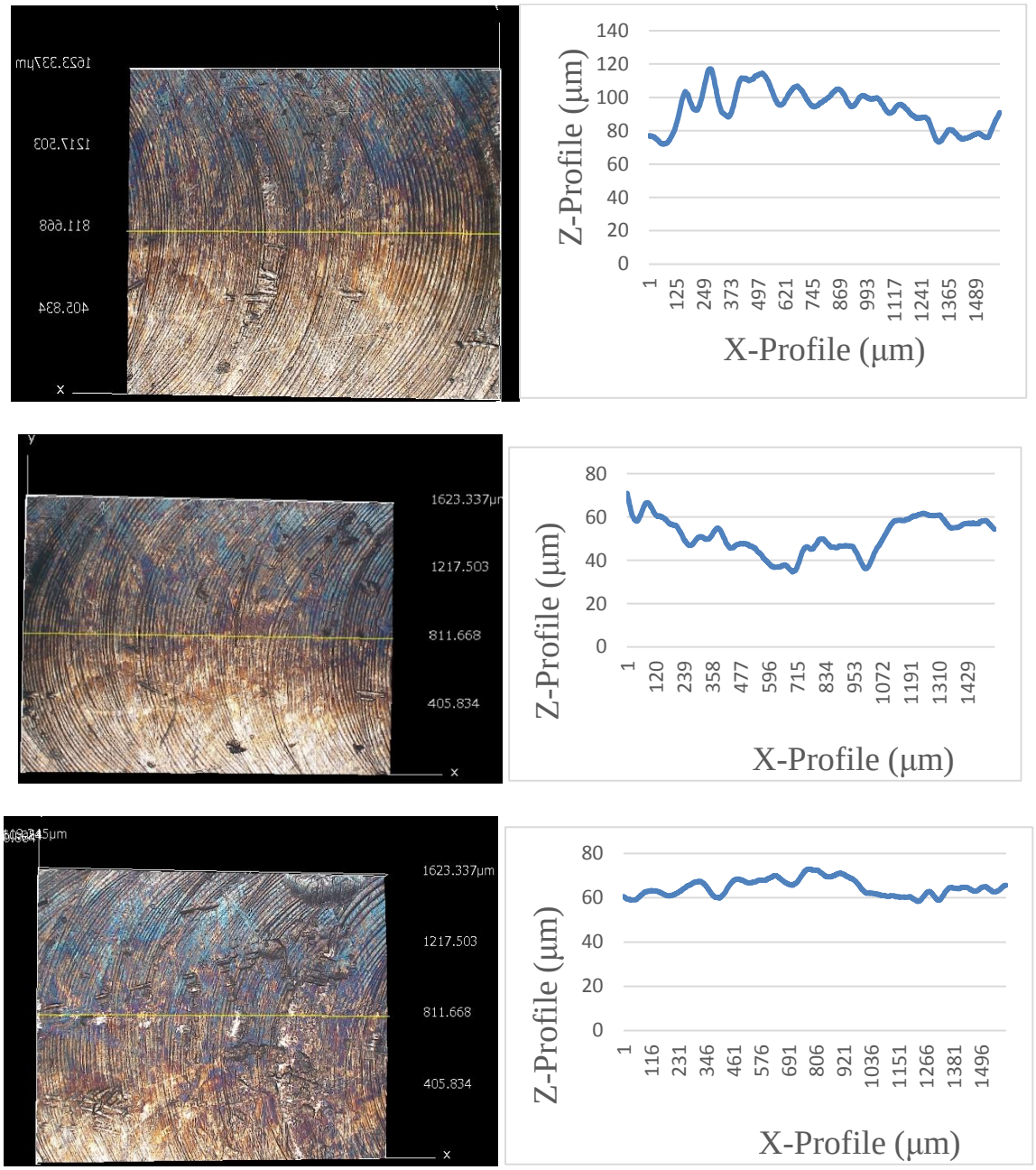

Figure 3-13 Surface profile of the laser melt before defect, surface profile of the laser melt on the defect and surface profile of laser melt after the defect

Table 3.4 Comparison of mean and standard deviation of surface mapping data of 304 stainless steel, laser surface melted sample and repaired sample

Sample	Mean of profile data (depth in microns)	Standard deviation
304 Stainless Steel	52.37	7.70
	46.43	6.57
	48.49	6.05
Laser Surface Melted Sample	127.83	5.8
	123.43	10.9
	91.04	5.6
Repaired Sample 1	93.2	11.88
	52.34	9.99
	64.63	3.73
Repaired Sample 2	91.51	8.24
	67.5	9.20
	86.83	8.66

The results included as part of Table 3.4 show the capability of LSM enabled repair in diverse situations.

- **LSM based repair ability:** Based on the repaired samples it is seen that LSM performed repair with consistently minimal variability across its entire length. The research's justification for the same is the minimal variation in the standard deviation that was topologically quantified.
- **Consistency of repair:** When the topological profile data of the repair sample 1 and repaired sample 2 are compared it seen that the mean and standard deviation closely match leading to the belief that in future this could transfer to a viable

repair option. All three zones namely the defect and the preceding and subsequent sections showed these trends validating the theory.

- **Baseline values for comparison:** The first two cases in the table are a study of defect less sample before and after LSM. This was used to assess the consistency of the laser and motion system to ensure that they did not produce any detrimental effects on the repair. As it can be seen by the consistency of their means and standard deviations they exhibited acceptable uniformity across all three zones.

Figure 3-14 Repaired sample

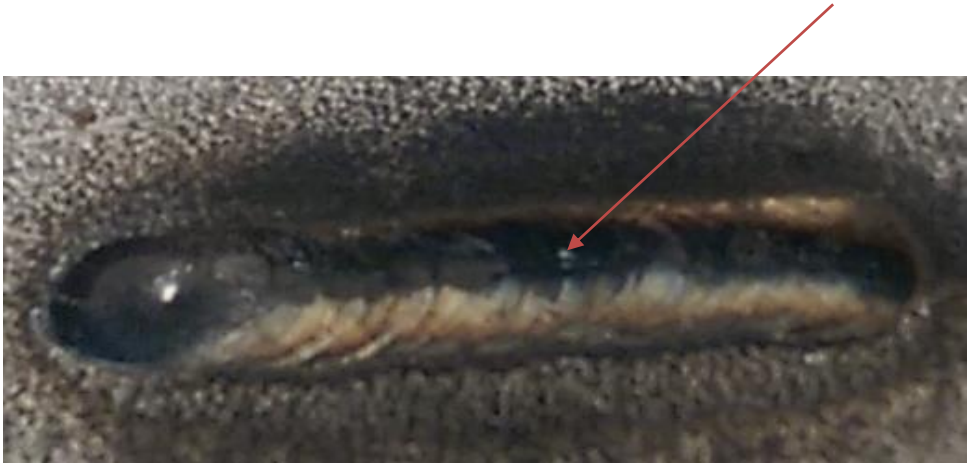

Figure 3-15 Repaired sample repetition

3.4.2 Repairing with Lower Melt Pool Depth. From the above experiments, it was observed that the standard deviations of the three cases were well within the limits. A similar sample was repaired at700W and 250 mm/min which would indicate a melt pool depth of 900 microns. This resulted in incomplete repair and the data is Figure 3-16. In case 2 a repair at 400 W and 100 mm/min with a melt pool depth of 660 microns was attempted. The resultant repair can be seen in Figure 3-17. The standard deviations of the surface plots for both cases are as seen in Table 3.5.

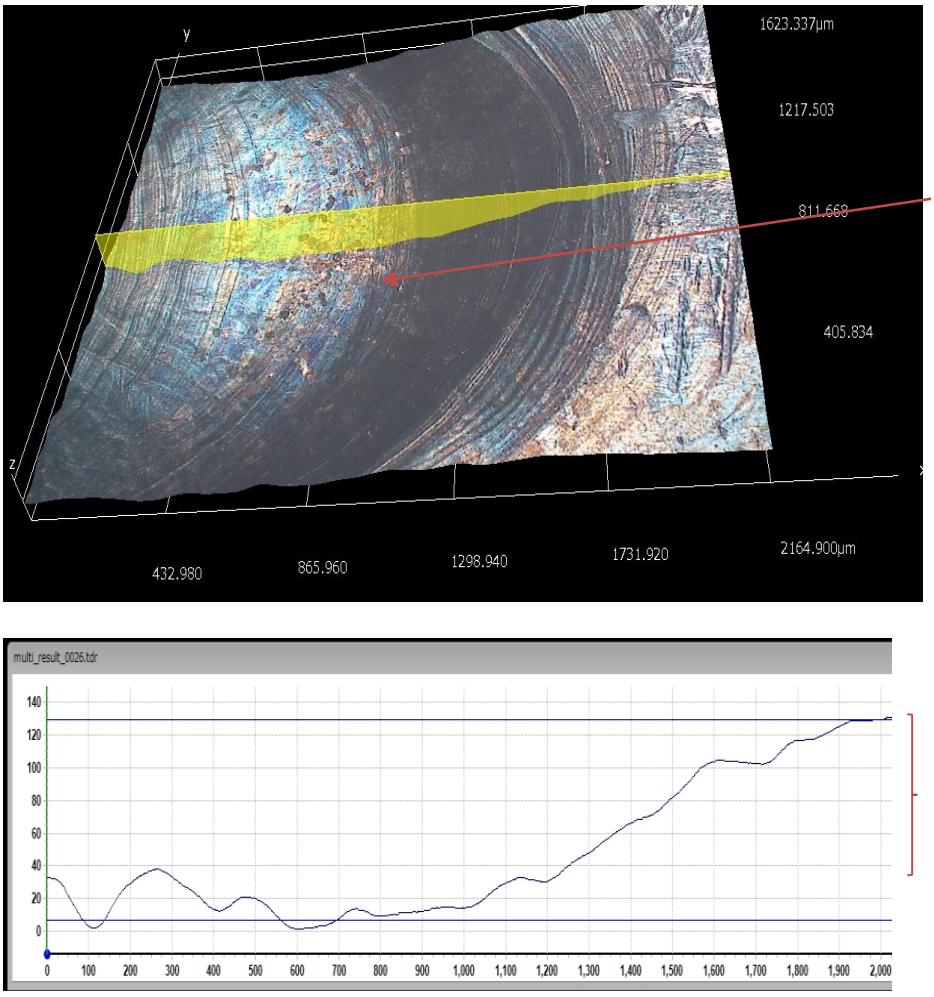

Figure 3-16 Surface profile and surface plot of case 1

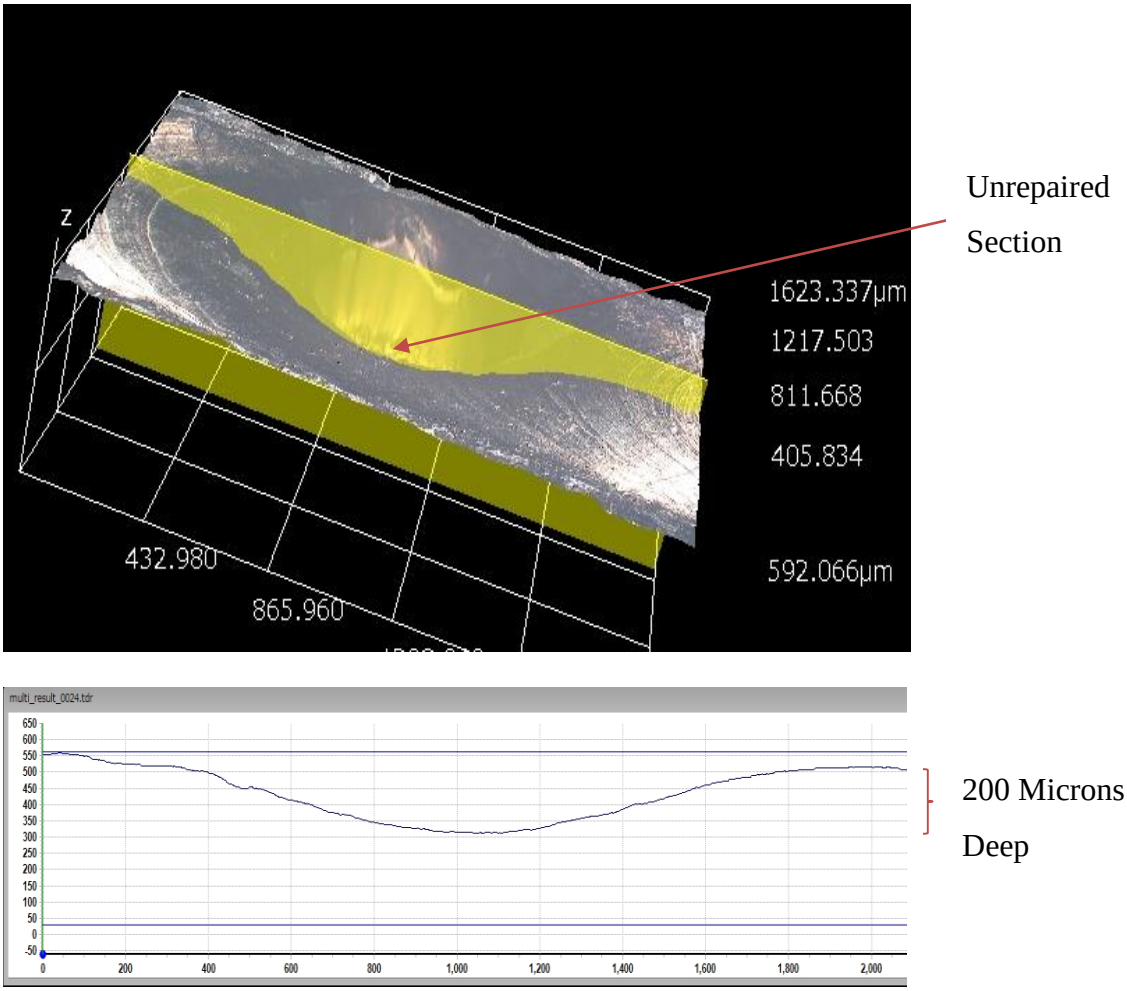

Figure 3-17 Surface profile and surface plot of case 2

Table 3.5 Standard deviation of surface plots for case 1 and case 2

Samples	**Standard Deviation**	**%Variation**
Case-1	49	82.65
Case-2	78	89.10

The creation and sustenance of a large melt pool is vital for repair to be successful in LSM. Certain situations like limited energy input or excessive travel speeds and

varying combinations of both lead to creation of melt pool of small volume and poor penetration. It is in situations like this that LSM repair could face difficulties as detailed by the cases 1 and 2. If both the process parameters were varied to produce poor melt pool characteristics which lead to poor repair. The variation as show by the excessive standard deviation in Table 3.5 is the justification for this conclusion**.**

3.5. SUBSURFACE REPAIR

3.5.1. Repairing a Subsurface Pore. Theoretically, the data generated from the experimentation and the numerical analysis can be used to determine the laser parameter values. Pores of three different sizes, 200 microns, 400 microns and 600 microns were prepared. Laser aided LSM was then used to repair the sample enabling a melt pool to form around the pore. The buoyancy forces in the system then push the bubble up to the surface where topological measurements reflect it as surface porosity. The top surface of the scanned samples with the void can be seen in Figure 3-18. The volume of the void created after repairing the 400 micron pore can be seen in Figure 3-19. The volume of the void created after repairing the 600 micron pore can be seen in the Figure 3-20. From the above data it can be observed that the volume of the void was always greater than the volume of the initial sub-surface defect that was to be repaired. This shows that the entire pore was filled. The excess volume might be due to the gas trapped between the two samples. The volumetric comparison between the pores and the volume of the void created can be seen in Table 3.6.

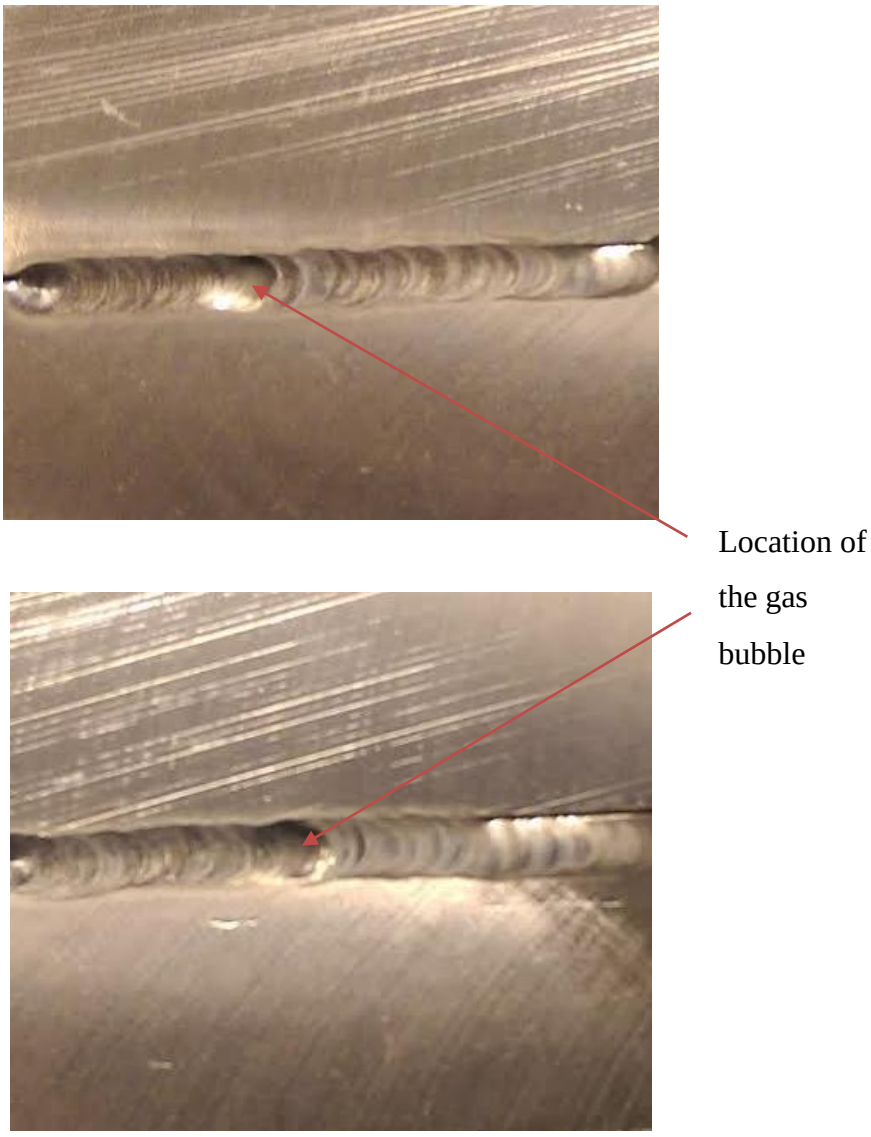

Figure 3.18 Void created by the escaping gas pore

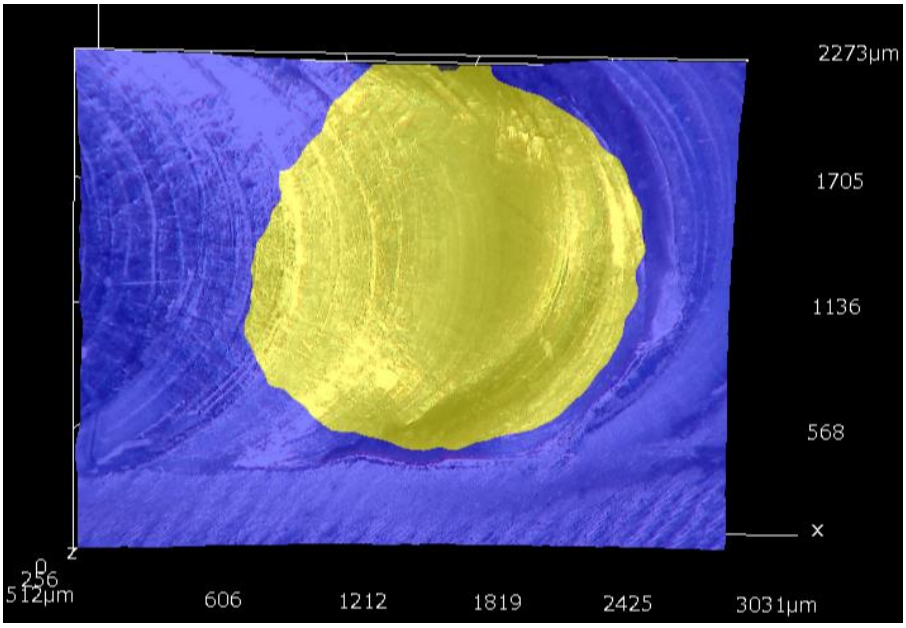

Figure 3-19 Microscopic image of the void created repairing 400 micron pore

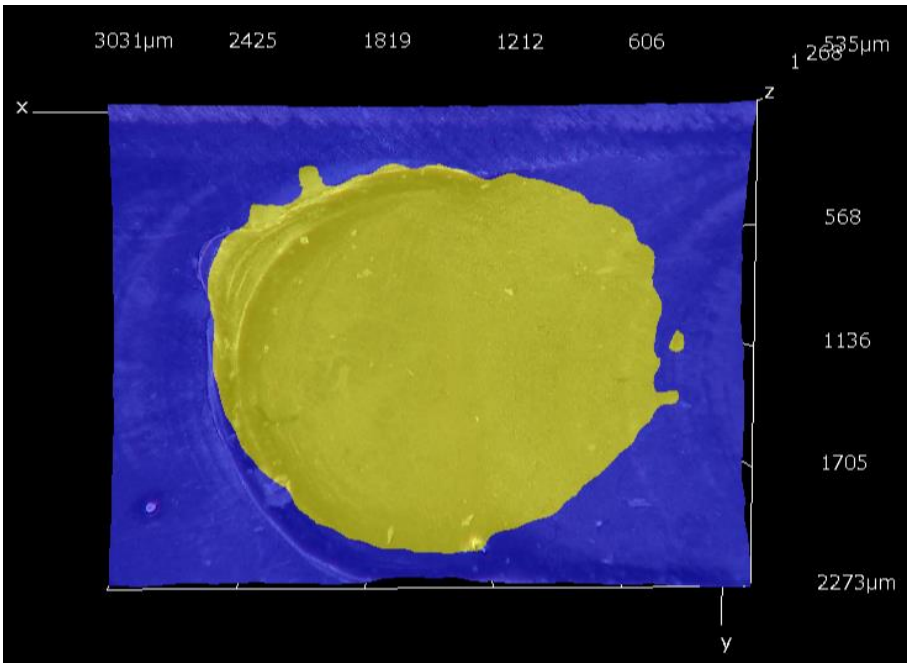

Figure 3-20 Microscopic image of the void created repairing 600 micron pore

Table 3.6 Volumetric comparison of the initial sub-surface defect and the surface porosity that was created during repair

Pore size (µm)	**Volume of the pore(μm^3)**	**Volume of the void(μm^3)**
200	31400000	48853537
400	125600000	157131500
600	282600000	312883587

From the above table it was observed that there is variation of 10-35% between the volume of the surface pore created and the actual volume of the pore. This might be combination of the gases trapped between the plates coupling with the defect pore volume to produce excessive differences.

3.5.2. Threshold Criteria for LSM Repair. LSM is a process of just energy input without the use of material to compensate for the defects volume. It was theorized that there exists a maximum porosity size beyond which LSM would prove to be unsuccessful. These next set of experiments were deployed to determine this threshold value and quantify LSM during unsuccessful repair situation. In case 1 the laser was scanned at 0.5mm offset from defect and it successfully repaired 65% of defect due to partial interaction with the pore whose 1mm size was not completely covered by the melt pool created. The optical microscopy image as seen in Figure 3-21 shows the topology of the pore, clearly distinguishing the repaired and unsuccessfully repaired sections. The volumetric comparison of the semi-filled pore can be seen in Table 3.7.

Side View of Pore

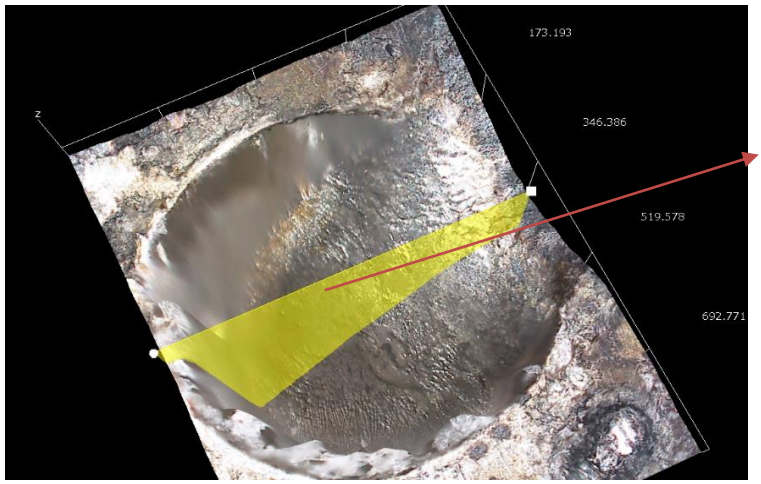

3D Profile of Pore

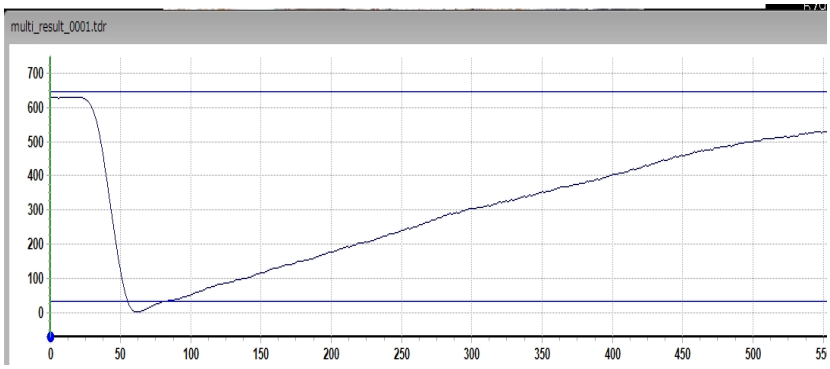

Z-Profile (µm)

X-Profile (µm)

Figure 3-21 Laser surface melting in case 1: Microscopic image of the pore, 3D surface map of the pore and surface plot of the pore

Table 3.7 Volumetric comparison of the semi-filled pore

Initial Volume of Pore (μm^3)	**Final Volume of Pore (μm^3)**	**Percentage Volume filled**
196250000	68687500	65

From the above table it was observed that only 65% percent volume of the sub-surface defect was filled. The partial interaction of the melt pool with the defect produced an unsuccessful repair. It is to be understood that this situation was created due to offset assumed as part of this LSM case. We also come to the conclusion that for the LSM to be successful the porosity has be located completely within the volume of the melt pool. If for some reason either the melt pool depth or travel path do not achieve this, partial or no repair will occur leading to unsuccessful LSM based repair.

These conclusions were reinforced by the results obtained as part of case 2 experiments. Here the LSM was offset by 1mm thereby almost missing the subsurface defect. The melt pool volume had minimal interaction with the subsurface defect producing partial repair as can be seen in Figure 3-22 and Table 3.8. The volumetric analysis in each of the cases also validate this with partially repaired volumes of 65% and 30% for case 1 and case 2 respectively.

Side View of Pore

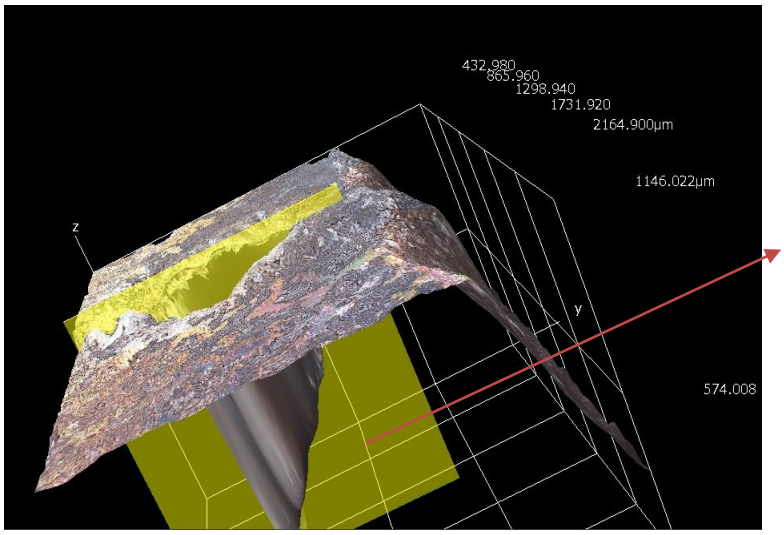

3D Profile of Pore

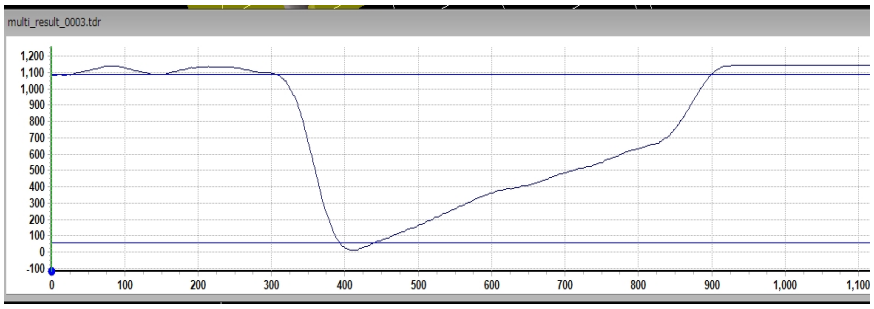

Z-Profile (µm)

X-Profile (µm)

Figure 3-22 Laser surface melting in case 2: Microscopic image of the pore, 3D surface map of the pore and surface plot of the pore

Table 3.8 Volumetric comparison of the semi-filled pore

Initial Volume of Pore (μm^3)	Final Volume of Pore (μm^3)	Percentage Volume filled
196250000	137375000	30

From the above table it was observed that only 30% percent volume of the sub-surface defect was filled. Again, this shows an unsuccessful repair of the sub-surface defect which reinforces the conclusion of case 1.

3.6. VOLUME TRANSPOSTION OF DEFECTS OBSERVED DURING REPAIR OF SURFACE DEFECTS

During the course of this research an interesting phenomenon was observed. It involved the transposition of a surface defect from one location on the substrate to another physical location. LSM was employed to repair the surface defect by starting from a point located 7 mm before the defect and ending 7 mm after the defect to simulate 15 mm of travel. After the experimental run a surface void was observed at the end of the travel while the original defect at the mid-section was noticed to disappear. This research leads to the conclusion that this void was created by the transposition of the defect from its initial location. This is justification of the fact that the volume of the defect in its original location (middle of the travel path) matches the volume of the void at the end of the travel. By creating and sustaining a stable melt pool that encompass the entire void transposition from one location to another was successfully achieved. This is an interesting phenomenon that was observed and can be employed to repair defects in locations which are difficult to reach for conversional repair solutions. The volume loss

observed is measured and quantified using topological maps generated by optical microscopy as shown in the following figures. Figure 3-23 shows the 3D topology and an indication of the measure of melt pool penetration cross-sectionally. The comparison of the volume removed to the volume loss observed is shown in Table 3.9. The quantified volume loss can be seen in Figure 3-24.

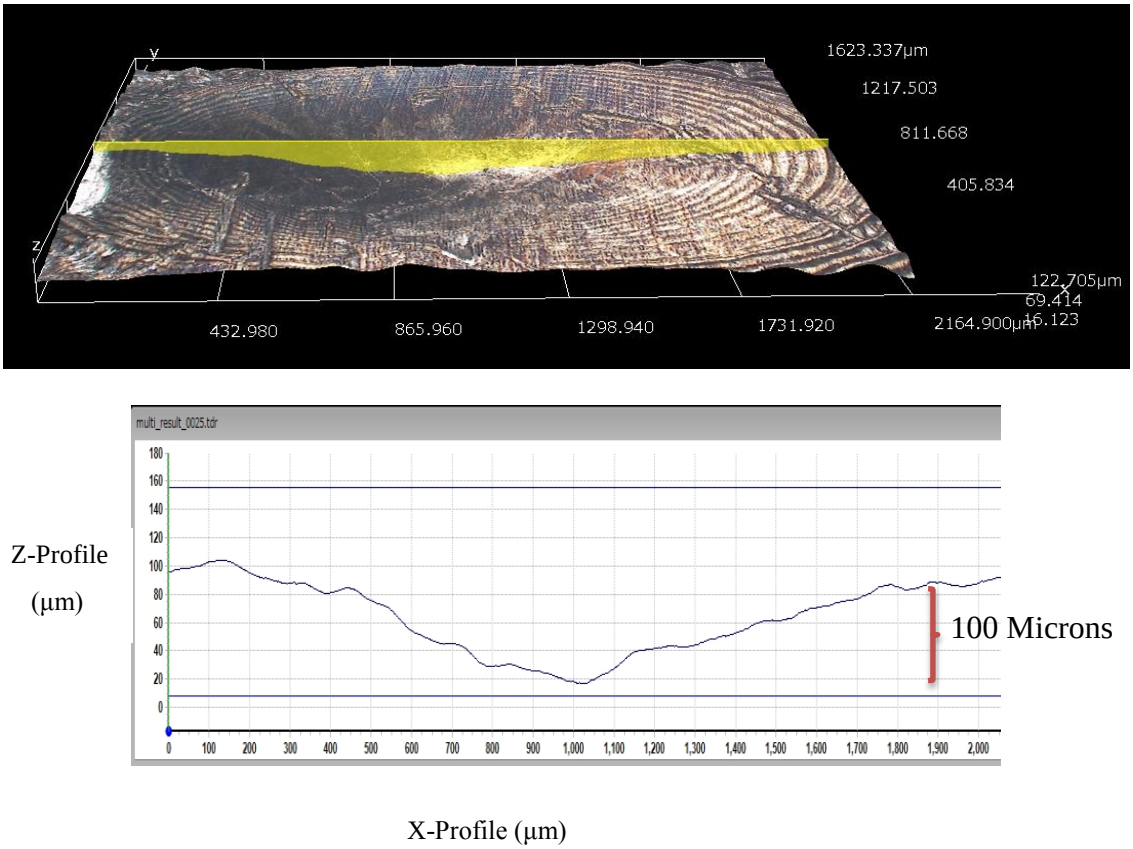

Figure 3-23 Volume loss observed during surface mapping in the case of surface defect repair

multi_result_0036.tdr

	Name	Center X [μm]	Center Y [μm]	Cross-S Area [μm^2]	Volume [μm^3]	Surface Area [μm^2]
1	Area/Volum	1083.127	812.345	2405056.724	181684653.679	2536897.317

Figure 3-24 Volume of the end hole

Table 3.9 Comparison of volume removed with observed volume loss

Volume Removed (μm^3)	Observed Volume loss (μm^3)	% Volume
196250000	181684653.679	92.57

The volume of the observed void is 92.5% of the initial surface defect created. This shows a successful transposition of the defect from its initial location to the end of the travel run.

4. CONCLUSION

The results from the experiments suggest that it is possible to use LSM as a viable repair solution for surface and subsurface defects specifically in metals. Numerical analysis was performed to understand the melt pool depth for various laser powers using the Gaussian heat flux equations. These results were compared with experimental analysis done by performing a planned series of experiments to determine the melt pool depth for various laser power and travel speed parameters. The numerical analysis results compared favorably with the experimental values.

The data generated from the numerical and experimental analysis was used to determine the process parameters for LSM enabled repair which were successfully employed to demonstrate the same. For the sake of brevity and clarity the entire analysis included in this thesis was performed on SS304 substrates of uniform dimensions. The surface repair was validated using the topological maps and their numerical quantification by computing the penetration depth of the melt pool. The means and standard deviations of this penetration depth had showed excellent repair characteristics in a multitude of cases. The experimentation was then progressed to determine the ideal process parameters for successful LSM repair and also determine the threshold values beyond which repair was poor. To minimize the effect of parameter interaction, base line studies of LSM samples were also performed. The research also qualitatively verified the repair to ascertain the presence of internal voids. This was done by cross-sectioning the sample using a wire-EDM to study the internal volume and validated the lack of internal defects.

LSM was successful in repairing subsurface defects if the laser travel path and the process parameters were properly identified. This was validated by observing the sectioned samples to ensure that no voids remained in the reformed melt pool zones. In certain situations where the melt pool did not suitably interact with the subsurface defect the LSM repair characteristics were noticed to be poor. Therefore path planning to ensure that the melt pool completely encompasses the surface and subsurface defects are critical to achieve acceptable repair characteristics. If the defect size exceed the melt pool size multipath planning is mandatory. Also there are certain defect volumes and depths beyond which LSM enabled repair will be unsuccessful. . Based on the study, the range of LSM enabled repair has been defined This 1kW fiber laser system with a beam diameter of 2mm can be used to repair defects up to 1.6 mm. In the case of subsurface defect LSM can be successfully employed to correctively repair defects of sizes 0.2-1mm located up to an mm below the surface.

5. FUTURE WORK

The aim of this research was to assess the feasibility of employing LSM as a viable repair option for metals. While the initial targets for the research has been achieved in the form of successful repair of surface and sub-surface defects, this research has the potential to be extended into a mass production environment. To achieve the same, this solution's prowess has to be proven across diverse manufacturing processes and material systems.

1. **Other steels**: During the course of this research LSM was proven on SS 304 samples. Hypothetically this can be extended into the repair of surface and subsurface defects in other steels and stainless steels. The existing market for these steels and stainless steels is extensive and proving the LSM concept will be an excellent start
2. **High performance metals and alloys**: These materials namely titanium alloys, inconels, tribaloys, etc. have thermal characteristics that are significantly divergent from stainless steels. Identifying the ideal process parameters combinations for each of these material systems to enable LSM repair would be a significant research achievement. Compiling these as repair process maps will also help the industry to achieve cost and performance targets.
3. **Healing of metals:** The content of this research focusses on manufactured surface and subsurface defects created using either milling or drilling. These processes remove material from the defect zone making it difficult to repair by redistributing material from the surrounding sections. But, in many cases this is not the only form of defect. Many defect situations also involve dents that are created by local geometric deformation and have not lost any material in the defect region. It is theorized that the

LSM enabled repair can be used to melt and recrystallize this local geometric deformation such that it can retain its original dimensional tolerance. Therefore this phenomenon of "healing" these local geometric distortions could fall under the purview of LSM repair.

4. **In-situ add-on for metal additive manufacturing:** Many metal additive manufacturing processes employ lasers to melt and deposit powders in layer-by-layer fashion. While they can produce complex geometries, they still suffer from the creation of porosities and cracks during deposition. This research if employed in conjunction with metal additive manufacturing could be an excellent repair option during deposition itself thereby significantly reducing resource wastage and improving part quality. If researched to its extent LSM enabled repair will be a valuable addition and make additive manufacturing a successful mass production process.

BIBLOGRAPHY

[1] John Ion, "Laser Processing of Engineering Materials, Principles, Procedures and Industrial Application", 2005, CSIRO, Australia

[2] Conde.A, Gracia. Ignacio and Damborenea. Juan de,Pitting, "Corrosion of 304 stainless steel after laser surface melting in argon and nitrogen atmospheres" Corrosion Science 2001, vol. 43 pp. 817- 828

[3] Cabeza.M, Castro.G, Merino.P, Pena.G and M Roman, "Laser surface melting: A suitable technique to repair damaged surface made in 14 Ni (200grade) maraging steel" Surface and Coating Technology 2012, vol 212 pp. 159-168

[4] Pinkerson.A.J, Wang.W, Li.L, "Component repair using laser direct metal deposition" Proceeding of the 35th International MATADOR Conference 2007, pp 345-35

[5] W.Peikarsha, M.Zubiak and Z.Saturnus, "Application of Abacus to analysis of the temperature field in elements heated by moving heat source" Archives of Foundry Engineering 2010, vol.10 pp.177-182

[6] G.Araya, G.Gutierrez, "Analytical Solution for a transient, three-dimensional temperature distribution due to a moving laser beam" International Journal of Heat and Mass Transfer 2006, vol 49 pp. 4124-4131

[7] Dimitrios Triantafyllidis and Lin Li, "Modelling of boundary Porosity formation in laser melting and re-solidification in ceramics" Journal of American Ceramic Society 2006, vol 89 pp. 1286-1294

VITA

Prudvi Teja Ravi was born in Visakhapatnam, Andhra Pradesh, the son of Rambabu Ravi and Mytreyi Ravi. He completed his undergraduate degree in Mechanical Engineering in Gitam University in 2012. He joined Missouri University of Science and Technology in August 2013 to begin his Master's in Manufacturing Engineering. During his study here, he worked as a Graduate Research Assistant in the Laser Aided Manufacturing Process laboratory.